ADVANCED SUSTAINABLE SYSTEMS
www.advsustainsys.com

Overcoming Electron Transfer Efficiency Bottlenecks for Hydrogen Production in Highly Crystalline Carbon Nitride-Based Materials

Ivo F. Teixeira, Nadezda V. Tarakina, Ingrid F. Silva, Nieves López-Salas, Aleksandr Savateev, and Markus Antonietti**

The hydrogen evolution reaction (HER) is a complex reaction involving many interdependent physicochemical steps. Highly ordered carbon nitride-based materials, such as Na-PHI and K-PHI, display some of the highest activities for H_2 evolution among the carbon nitride-based materials, due to their electronic properties, but also the presence of cyanimide terminations, which favors the charge transfer for the Pt cocatalyst nanoparticles (NPs). For such highly optimized semiconductor structures, the necessity to control and improve other steps of the photocatalytic process becomes essential, in particular the poor electron transfer from the Pt NPs to the protons in solution over the Helmholtz or Stern layer. Taking highly ordered Na-PHI as a test material, the influence of water-dissolved alkali cations on the HER is systematically studied and it is experimentally verified that the electron transfer from the Pt NPs to the protons in solution limits the efficiency of heterogeneous carbon nitride-based catalysts. This paper explains how hydrated alkali cations influence electron transfer and are able to boost the H_2 evolution rate of the same Na-PHI from 2401 up to 5330 µmol h^{-1} g^{-1} with an apparent quantum yield of 13% at 420 nm.

1. Introduction

Water splitting photocatalyzed by semiconductors irradiated by sun-light promises the production of clean and renewable hydrogen gas to supply energy and feedstock for hydrocarbon and alcohol production.[1] Despite storage of hydrogen gas is very challenging, it is undeniable that it will have an essential role in the replacement of fossil fuels in the future. Nonfossil hydrogen sources will be essential to make CO_2 reduction technology sustainable, since nowadays 96% of commercial hydrogen comes from fossil fuels.[2] Among the renewable sources of hydrogen gas, certainly, sun-light-driven water splitting is one of the most promising. The fundamental steps of efficient photocatalytic water splitting include photon absorption, charge separation, and transfer of photogenerated electrons and holes to electrochemical interfaces to drive surface chemistry, such as the formation of the H—H bond after proton reduction.[3]

Commonly, in studies that deal with water splitting photocatalyzed by semiconductors, hole or electron scavengers are often added to remove one charge carrier efficiently from the photocatalyst. This approach facilitates the investigation of the complementary oxidation/reduction reaction (e.g., proton reduction to H_2 and water oxidation to O_2).[4] The scavenging process can, however, create a strong kinetic asymmetry in the carrier extraction from the light absorber, resulting in the accumulation of one type of charge,[5,6] as detailed in **Figure 1**. This charge accumulation process may generate bottlenecks in the hydrogen evolution reaction (HER) photocatalyzed by carbon nitride-based materials. As demonstrated by Durrant and co-workers the trapped charges promote an increment in the e^-/h^+ recombination rate constant (k_3), resulting in lower performance. However, this is only one of the possible limiting steps in the HER, and we will show that current limitations are also beyond the interface of the semiconductor.

Recently, carbon nitride-based materials have attracted attention due to their many merits in terms of visible light response,[7] easy-modified textural/electronic structure,[8,9] and great photochemical stability.[8,10] Although polymeric carbon nitride (PCN) standing out as the most investigated carbon nitride-based material in the HER, unfortunately, pure PCN, without modification/optimization of its structure and properties, displays a very limited activity even in the presence of scavengers.[11] The synthesis of carbon nitride materials in the presence of an inorganic salt, such as NaCl, KCl, and LiCl, which can be molten or not in the synthesis conditions, lead to a range of highly ordered carbon nitride-based materials with improved efficiency in the HER.[12]

I. F. Teixeira
Department of Chemistry
Federal University of São Carlos
São Carlos, SP 13565-905, Brazil
E-mail: ivo@ufscar.br

I. F. Teixeira, N. V. Tarakina, I. F. Silva, N. López-Salas, A. Savateev, M. Antonietti
Department of Colloid Chemistry
Max Planck Institute of Colloids and Interfaces
Am Mühlenberg 1, D-14476 Potsdam, Germany
E-mail: office.cc@mpikg.mpg.de

The ORCID identification number(s) for the author(s) of this article can be found under https://doi.org/10.1002/adsu.202100429.

© 2022 The Authors. Advanced Sustainable Systems published by Wiley-VCH GmbH. This is an open access article under the terms of the Creative Commons Attribution-NonCommercial License, which permits use, distribution and reproduction in any medium, provided the original work is properly cited and is not used for commercial purposes.

DOI: 10.1002/adsu.202100429

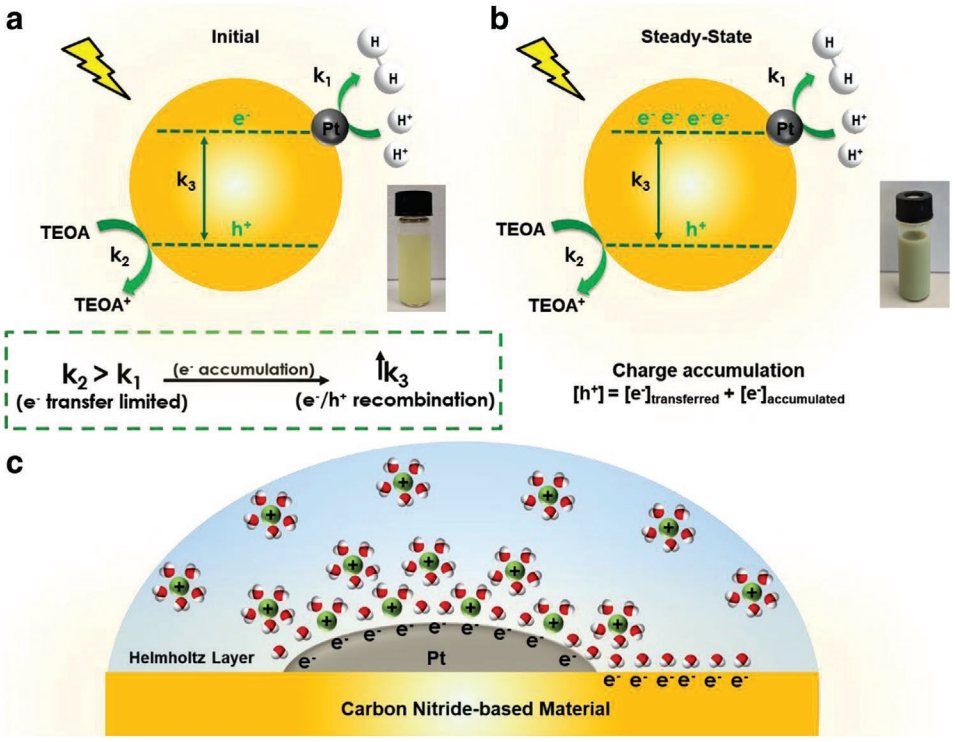

Figure 1. a) Schematic representation of the charge accumulation process in carbon nitride-based materials, where k_1 represents the electron transfer rate constant (proton reduction), k_2 is the h^+ scavenging rate constant and k_3 represents e^-/h^+ recombination rate constant. b) Charge accumulation in the steady-state and c) Schematic representation of the Helmholtz double-layer generated by the negatively charged surface.

As mentioned above, a successful HER depends on three consecutive processes: 1) photon absorption, 2) charge separation, and 3) transfer of photogenerated electrons and holes to surface states, cocatalysts, and to the solution-based reactant. The third step is particularly important, as it involves a series of other processes. Hydrogen evolution reactions performed in the presence of hole scavengers will not be limited by the hole extraction (k_2), thus the electron transfer step can be optimized, independently. The electron transfer process is then dependent on the effective transfer of the electrons to the cocatalyst (here Pt, essential for the reaction). For example, Lotsch et al. have shown that PCN functionalized with extra cyanamide is 12- to 16-fold more active in HER. The authors claimed that the increment of the H_2 evolution is owed to the more effective charge transfer between PCN and the Pt nanoparticles (NPs). Once the electrons have been moved to the Pt nanoparticles (NPs), an effective cocatalyst has to mediate the reaction between these electrons and the protons in solution. We usually assume that this reaction is not a rate determining step, but colloids, especially in water, are protected by tight and strongly bound counterions in Helmholtz-layer (Figure 1c), counterions and ions in Stern layer, and these ion layers act as polarizing complex resistance to the protons.

Some of the carbon nitride-based materials photocatalysts, with strong oxidation potential, under irradiation, can undergo a charge accumulation process (Figure 1).[4,5,13,14] The charge accumulation is due to the kinetic asymmetry of the carrier extraction from the photocatalyst. For the strongly oxidizing carbon nitride-based materials in the presence of a h^+ scavenger, such as triethanolamine (TEOA), the oxidation reaction rate constant (k_2) is significantly higher than the electron transfer rate constant (k_1), leading to the accumulation of electrons. This process can be easily noticed by the photocatalyst color change from yellow to greenish (Figure 1a,b). Durrant et al. have demonstrated that these stored charges increase the e^-/h^+ recombination rate constant (k_3), resulting in lowered efficiency.[4,13] After few minutes, the system with the excess of electrons reaches an equilibrium, where positive and negative charges vanish with the same speed. In summary, the H_2 evolution reaction in presence of a hole scavenger is limited by the electron transfer to the reactants, and any increment of it will favor chemical use of the separated e^-/h^+ pairs and consequently lead to higher quantum efficiencies.

Herein, we systematically studied the influence of alkali cations dissolved in the water phase on HER. Varying the nature of the alkali cation evidenced that it is caused by the activation of the water hydrogen-bond network by interacting with the negatively polarized oxygen. This leads us to hypothesize that electron transfer from the Pt NPs to the protons in solution is rate limiting the efficiency of heterogeneous carbon nitride-based catalysts. This hypothesis was experimentally verified by detailed photocatalytic tests and time-resolved photoluminescent experiments. Thus, it was revealed that the current bottleneck for highly efficient heterogeneous carbon nitride-based materials is indeed the electron transfer from the Pt NPs cocatalyst to the proton in solution (alternatively described as the proton transfer through the Helmholtz layer to the Pt-atoms at the surface). This new find was applied to the rational design of

© 2022 The Authors. Advanced Sustainable Systems published by Wiley-VCH GmbH

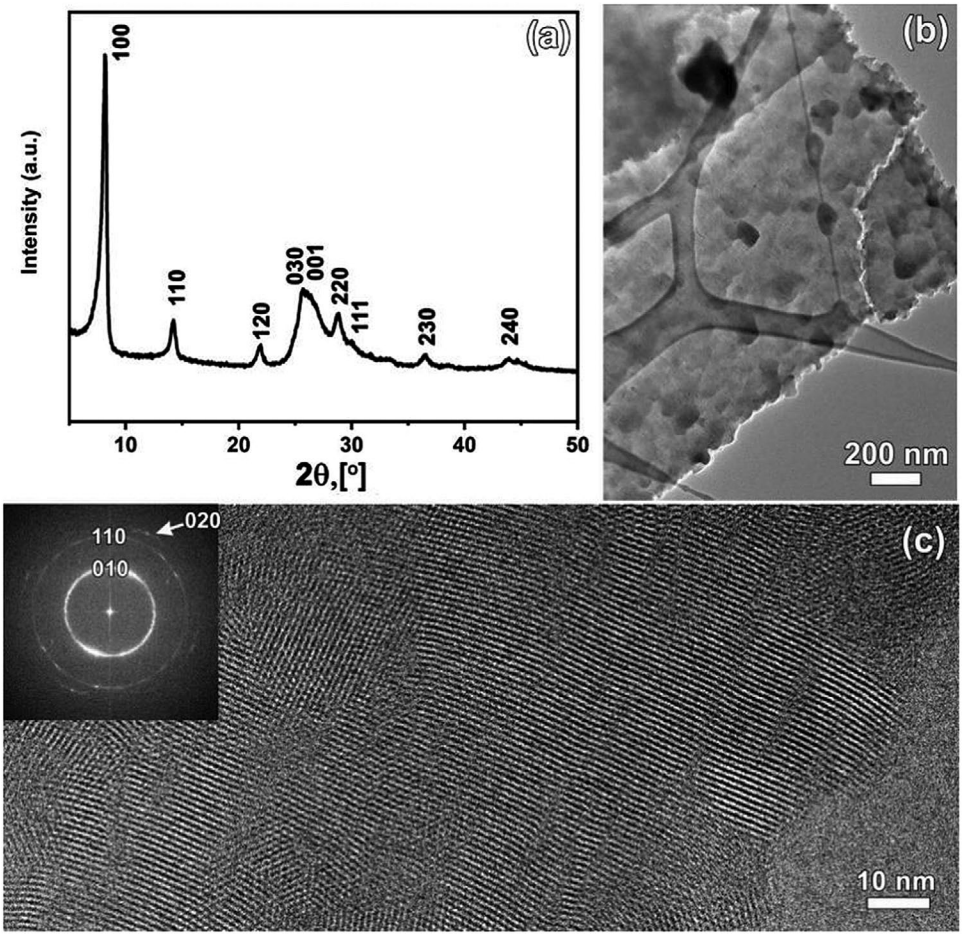

Figure 2. a) X-ray powder diffraction pattern of Na-PHI. b) Overview TEM image of a typical Na-PHI flake and c) HR-TEM images of Na-PHI, the corresponding fast Fourier transformation (FFT) is given in the inset (left).

the electrochemical double-layer in water leading to greater H_2 evolution rates and apparent quantum yields (AQYs).

2. Results and Discussion

2.1. Sodium Poly(heptazine imide) (Na-PHI) Characterization

Highly crystalline Na-PHI was obtained by heating a mix of melamine and NaCl at 600 °C, as described in the Experimental Section. The crystal structure of Na-PHI was analyzed using X-ray powder diffraction (XRD) and high-resolution transmission electron microscopy (HR-TEM) (**Figure 2**). TEM images show the formation of the big flakes of Na-PHI consisting of nanometer-size crystalline domains (Figure 2b,c). Both XRD and selected area electron diffraction patterns were indexed in a hexagonal lattice (space group *P31m*) with the unit cell parameters a = 14.3739(1) Å, c = 3.36681(6) Å in agreement with our previous reports. The PHI layers are aligned directly on top of each other forming continuous channels along the c direction (AAA stacking).[6] Analysis of both HR-TEM and SAED data shows that nanocrystalline domains tend to be preferentially oriented in the flack along the c direction of the structure, but possess rotational disorder in the *ab* plane.

The Na-PHI synthesized here displays a band at 2179 cm^{-1} in the Fourier transform infrared (FTIR) spectrum (**Figure 3**a), which evidences the presence of cyanamide groups.[15] Typical bands of heptazine-based carbon nitrides are also observed, e.g., 1107, 985, and 796 cm^{-1}.[16] It is also worth noting the band in 1206 cm^{-1} related to aromatic amine C–N stretching.[16]

The bandgap of the sample was determined by applying the method reported by Makuła et al.[17] from the UV–vis diffuse reflectance absorption spectra (Figure 3b). The obtained bandgap was 2.78 eV, which is not very different compared to PCN (2.7 eV)[18] and others heptazine-based materials, such as K-PHI (2.67 eV). The bands' position of the Na-PHI was estimated from the Mott–Schottky plots (Figure S2a, Supporting Information) and the values of 2.54 and −0.24 V versus SHE were obtained for the valence band and conduction band (Figure S2b, Supporting Information), respectively.

2.2. The Alkali Cation Effect

The highly crystalline, layered Na-PHI already displays an excellent activity in H_2 evolution, around 2400 μmol h^{-1} g^{-1} of H_2 (**Figure 4**b), which can be further improved by adding alkali

© 2022 The Authors. Advanced Sustainable Systems published by Wiley-VCH GmbH

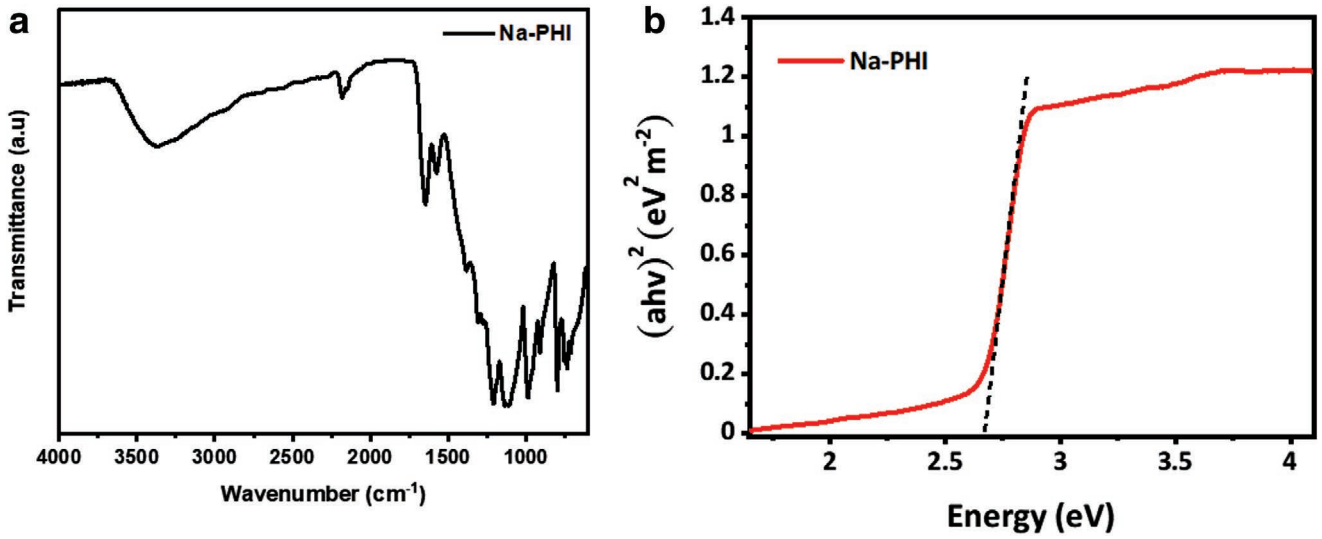

Figure 3. a) FTIR comparison of long-layered Na-PHI. b) $(ahv)^2$ versus hv curve of long-layered Na-PHI, displaying a bandgap of 2.78 eV. The optical bandgap was determined by the method described by Makuła et al.[17]

salts in the reaction media (Figure 4a,b). Zhang et al. reported an increment of H_2 evolution rate in modeled seawater (3 wt% NaCl) for highly crystalline carbon nitride-based materials, while this effect was not observed for PCNs with their much higher reduction potentials.[19] The authors attributed the salt effect to the chloride anion oxidation in the Helmholtz layer of the photocatalyst. Despite the redox potential of chlorine (≈1.36 V vs SHE) being within the oxidative potential of the generated holes,[20] it is significantly higher than the TEOA oxidation potential (0.57–0.82 V), and again the structure of the Helmholtz layer and its permeability for TEOA must be discussed. A similar effect was reported by Wu and co-workers to alkali halide salts in seawater, and the author attributed the promoting alkali effect to the coordination to the TEOA, thus facilitating its contact with the carbon nitride-based material.[21] As the oxidation step takes place with a faster rate constant (k_2), it is not the limiting step for the hydrogen evolution reaction, consequently, it is very unlikely that the alkali promoting effect previously reported is related to the alkali cation coordination to the TEOA molecule.

In order to test the influence of the chloride anion in our reaction system, we performed the reaction in the presence of 0.25 mol L^{-1} of NaCl and NaF (Figure 4c). Fluoride anions have a redox potential (≈2.87 V vs SHE) significantly higher than that of chloride anion.

Therefore, halogen shuttle can be excluded, and the rate should decrease. However, we observe exactly the opposite. In the presence of NaF the Na-PHI H_2 evolution rate was further improved to 4340 μmol h^{-1} g^{-1} against 3224 μmol h^{-1} g^{-1} for the sample in NaCl solution. This result indicates that the promoting effect of salts in the HER is cation-related and not anion-related, as previously reported. The higher activity observed in NaF might be related to a negative effect promoted by the competition of the Cl^- anions for the oxidation site, as demonstrated by Markushyna et al. highly ordered carbon nitride materials can oxidize Cl^- ions under the reaction conditions.[20]

As shown in Figure 4d, the AQY for Na-PHI tested in three different wavelengths follows very well the Na-PHI absorption spectra. The sample Na-PHI was tested in the presence of 1 mol L^{-1} of LiCl irradiated in 420, 465, and 525 nm, the results were 12.9%, 0.8%, and 0.01%, respectively. Also, in the presence of 1 mol L^{-1} of LiCl, Na-PHI shows a significantly higher activity compared with Na-PHI without added salt (Figure 4a).

Furthermore, the H_2 evolution was evaluated in different concentrations of LiCl, as shown in **Figure 5**. The Na-PHI activity increases from 3373 up to 5330 μmol h^{-1} g^{-1} when the LiCl concentration is incremented from 0.25 to 1.0 mol L^{-1}. The LiCl in solution does not seem to affect the stability of the Na-PHI, which displays high activity in HER for hours in consecutive cycles (Figure 4a). The XRD patterns of the sample in LiCl before and after HER are shown in Figure S1 of the Supporting Information, and no significant change is noticed, especially for the peaks 100, 110, and 120, evidencing the integrity of the Na-PHI structure. The region between 25° and 30° displays some peak broadening (Figure S1, Supporting Information), which possibly is related to the exfoliation of the sample during the reaction.

2.3. Mechanism Investigation

The highly crystalline Na-PHI was then tested in the presence of different alkali chlorides. As shown in Figure 4b, LiCl displays the higher H_2 evolution rate (3373 μmol h^{-1} g^{-1}) followed by NaCl, KCl, and CsCl, respectively. The effect of the alkali metal cation observed here is proportional to the hydration energy of the alkali salts. As previously reported for electrochemical H_2 evolution in basic media, alkali salts display a promoting effect in the reaction proportional to its hydration energy.[22,23] The larger the hydration energy of the alkali metal cation, the stronger is the surrounding H-bridge network, and the larger the electrochemical H_2 evolution activity.[23] The alkali metal cation activates the H—OH bond by pulling the

© 2022 The Authors. Advanced Sustainable Systems published by Wiley-VCH GmbH

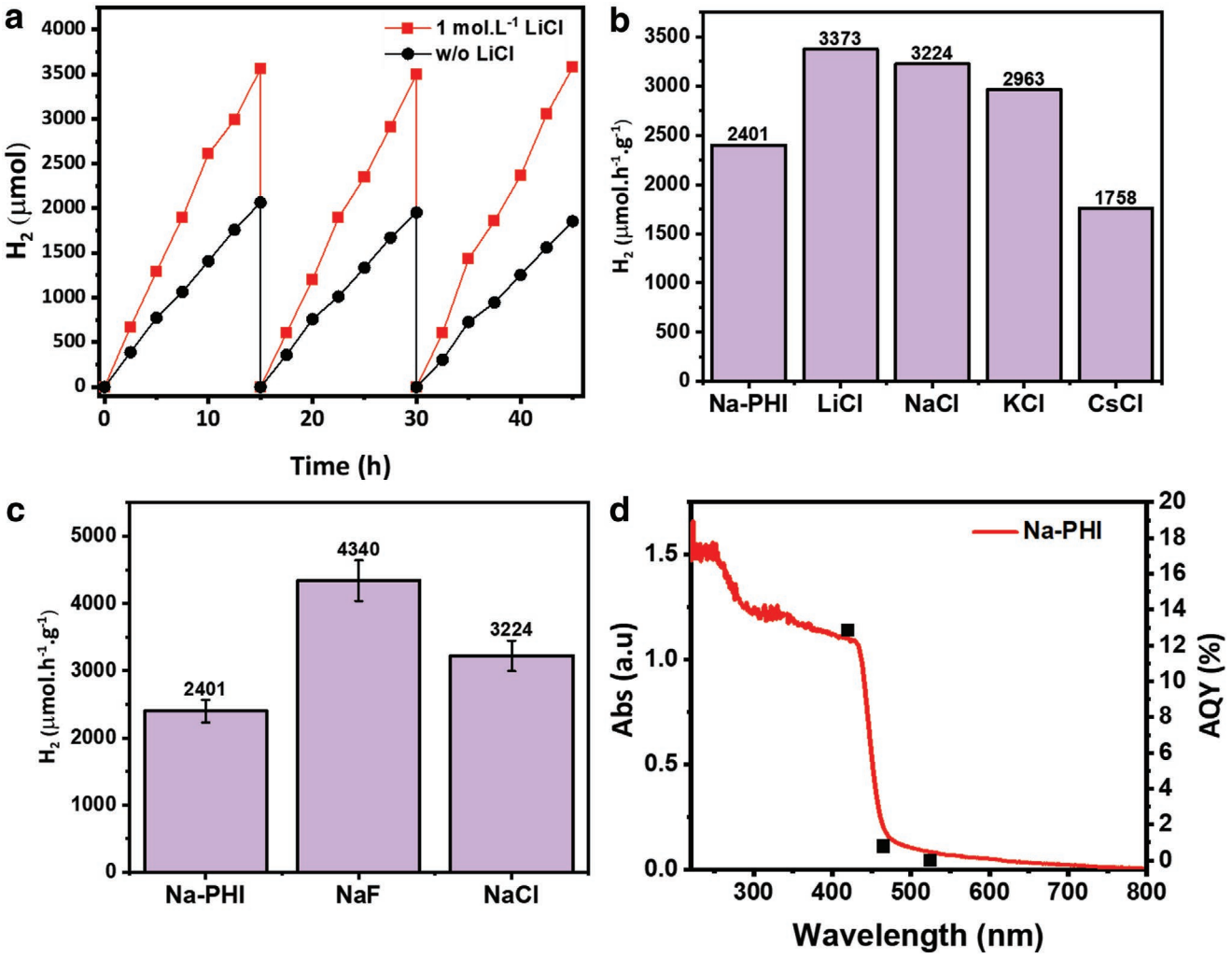

Figure 4. a) Time course of the hydrogen evolution reaction for 50 mg of Na-PHI with and without LiCl in solution (1.0 mol L^{-1}). b) Photocatalytic H_2 evolution rates of Na-PHI in the presence of different alkali salts (0.25 mol L^{-1}). c) Photocatalytic H_2 evolution rates of Na-PHI in the presence of 0.25 mol L^{-1} of NaF or NaCl. d) UV–vis diffuse reflectance absorption spectra (DRS) of Na-PHI and its apparent quantum yield (AQY) in H_2 evolution reaction under irradiation with different wavelengths in the presence of LiCl (1.0 mol L^{-1}).

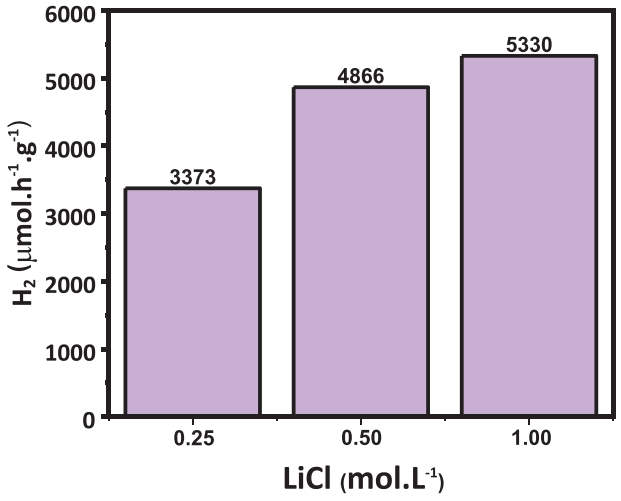

Figure 5. Photocatalytic H_2 evolution rates for long-layered Na-PHI in the presence of different concentrations of LiCl.

negatively charged oxygen (**Figure 6**b) and makes the proton more mobile, also expressed by higher acidity. The proton can now pass to the Pt-nanoparticle surface and can be combined with a waiting electron to be chemisorbed as reduced hydrogen on the platinum cocatalyst surface, while the left hydroxide in the hydration shell can pump further protons to the surface along with the cation.[23]

The mechanism of the electrochemical HER in alkaline media is typically treated as a combination of three elementary steps: the Volmer step (water dissociation) and formation of a reactive intermediate adsorbed hydrogen ($2H_2O + Pt + 2e^- \leftrightarrows 2Pt\text{-}H_{ad} + 2OH^-$), followed by the Heyrovsky step ($H_2O + Pt\text{-}H_{ad} + e^- \leftrightarrows Pt + H_2 + OH^-$) or the Tafel recombination step ($2Pt\text{-}H_{ad} \leftrightarrows 2Pt + H_2$).[22] A rigorous analysis of the adsorption of protons in the metal surface, despite being very interesting, lies beyond the scope of the present discussion. However, we can safely assert that in basic conditions the water dissociation has a key role in the reaction, which is being facilitated by the presence of alkali cations in the medium. This

© 2022 The Authors. Advanced Sustainable Systems published by Wiley-VCH GmbH

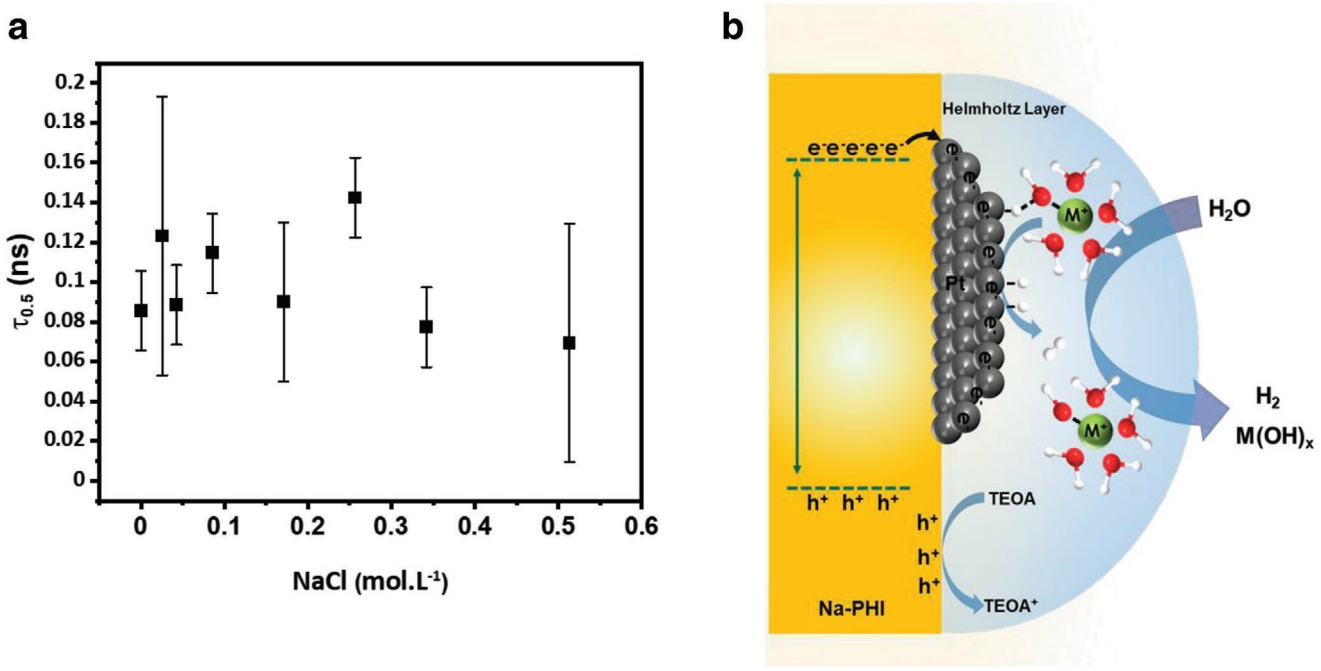

Figure 6. a) Half-time decay of Na-PHI in the presence of different concentrations of NaCl at the same conditions as the HER was conducted. b) Schematic representation of the alkali cation effect in the H_2 evolution reaction, showing the activation of O—H bond promoted by the alkali metal.

is undoubtedly indicated by the trend observed in our experiments, which demonstrated that as stronger the hydration energy of the cation higher the HER activity. In both possible mechanisms to the H_2 formation, the alkali cation effect seems positive, it might be acting not only in the Volmer step (essential in both mechanisms), helping to promote the water dissociation, as well as it might have a positive effect in the Heyrovsky step, facilitating the stabilization of the OH^- produced.

In order to confirm that the alkali metal cation promotion effect is related only to the electron/proton transfer step of the H_2 evolution reaction, time-resolved photoluminescence experiments were conducted. The half-time decay of Na-PHI was monitored under the reaction conditions in the presence of different concentrations of NaCl. As shown in Figure 6a, the salt concentration does not seem to influence the half-time decay for the Na-PHI. In other words, the ions in solution do not influence directly the e^-/h^+ recombination rate, but act far from the semiconductor part down the electron transfer processes.

This bottleneck caused by the limitation in the electron transfer from Pt NPs to protons was already demonstrated by Durrant et al.,[4] who addressed this issue by adding methyl viologen (MV^{2+}) as an electron mediator to the reaction. The authors reported a 30% efficiency gain for cyanamide surface-functionalized melon-type carbon nitride ($^{NCN}CN_x$) in the presence of MV^{2+}, due to the removal of trapped electrons, which may disfavor the H_2 production.[4,13] When no alkali salt is added we notice a similar gain with the addition of MV^{2+}. We also investigated the effect of added MV^{2+} for Na-PHI with and without salts in solution, in order to evaluate the effect of the trapped charges under our reaction conditions. As shown in **Figure 7**, our reaction system in the presence of MV^{2+} showed only a negligible increment in H_2 evolution rate from 3224 to 3365 μmol h^{-1} g^{-1}, indicating that in the presence of alkali the electron transfer from Pt NPs to protons is promoted automatically diminishing the counterproductive effect of the trapped electrons.

The use of alkali cations in solution, as demonstrated here, proved to be effective enough to improve the electron transfer from Pt NPs to protons, consequently increasing the overall activity of the layered Na-PHI. Under optimized conditions, Na-PHI displayed an excellent AQY of 13% at 420 nm (Figure 4d). Due to the narrow absorption spectra of Na-PHI in the visible range, the AQY drops drastically to 0.16% at 465 nm, as shown in Figure 4d.

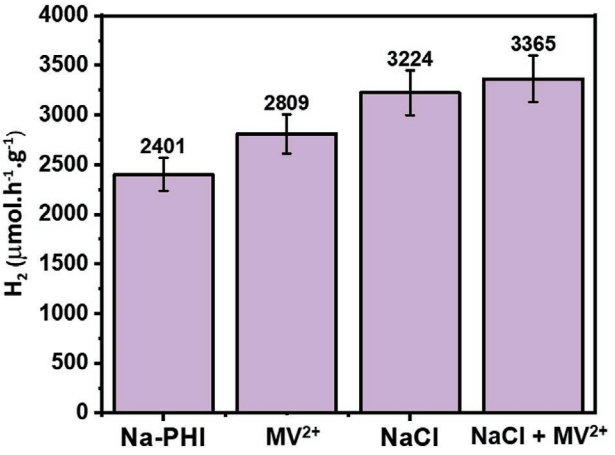

Figure 7. Photocatalytic H_2 evolution rates for long-layered Na-PHI in the presence of 0.25 mol L^{-1} NaCl and/or 10 μmol of MV^{2+}.

© 2022 The Authors. Advanced Sustainable Systems published by Wiley-VCH GmbH

3. Conclusions

In summary, we have demonstrated here a promoting alkali cation effect that follows the hydration energy for the alkali cation ($Li^+ > Na^+ > K^+ > Cs^+$). We proved that this effect is caused by the activation of the H—OH bond by pulling the negatively charged oxygen. More importantly, for the first time, it was verified that the current bottleneck for highly efficient heterogeneous carbon nitride-based materials in the HER is indeed the poor electron transfer from the Pt NPs cocatalyst to the proton in solution (alternatively described as the proton transfer through the Helmholtz layer to the Pt-atoms at the surface). This finding opens a new horizon in the optimization of highly efficient photocatalysts to HER, indicating that the rational design of the electrochemistry double-layer in water is of paramount importance to improve activity in HER.

4. Experimental Section

Synthesis of Na-PHI: Na-PHI was prepared by thermocondensating a mixture of melamine (10 g) with NaCl (100 g) previously grounded in a ball mill for 5 min. The reaction mixture in an alumina crucible (100 mL) was heated up in an oven under constant nitrogen flow (1 L min^{-1}) to 600 °C with a heating rate of 138 °C h^{-1}, held at 600 °C for 4 h, and then allowed to cool down. The product was removed from the crucible, washed with deionized water (1 L), isolated by centrifugation (9000 rpm, 5 min), and then thoroughly washed with deionized water on the filter (1 L). After that, it was dried overnight in an oven at 60 °C.

Characterization: The X-ray powder diffraction patterns were recorded on Bruker D8 Advance diffractometer equipped with a scintillation counter detector with Cu Kα radiation (λ = 0.15418 nm) applying 2θ step size of 0.05° and counting time of 3s per step. Steady-state UV–vis absorption spectra were acquired using Shimadzu UV 2600 in diffuse reflectance mode. The bandgap was calculated by a linear fit of the valence region (0–5 eV). Fourier transform infrared attenuated total reflectance spectra were recorded on a Varian1000 FT-IR spectrometer equipped with an attenuated total reflection unit with diamond, with a resolution of 4 cm^{-1}. Elemental combustion analysis was accomplished using a Vario Micro device. Inductively coupled plasma-optical emission spectrometry was conducted using a Horiba Ultra 2 instrument equipped with photomultiplier tube detector.

For HR-TEM observations, a suspension of the sample in ethanol was sonicated for 10 min and then drop-casted to a Cu grid with lacey carbon support and dried for 5 min. The TEM study was performed using a double Cs corrected JEOL JEM-ARM200F (S) TEM operated at 80 kV and equipped with a coldfield emission gun.

Electrochemical measurements were conducted with a BAS Epsilon Electrochemical System in a conventional three-electrode cell, using a Pt plate as the counter electrode and an Ag/AgCl electrode (3 M KCl) as the reference electrode. The working electrode was prepared on F-doped tin oxide (FTO) glass that was cleaned by sonication in ethanol for 30 min and dried at 353 K. The boundary of FTO glass was protected using Scotch tape. The 3 mg sample was dispersed in 1 mL of water by sonication to get a slurry mixture. The slurry was spread onto pretreated FTO glass. After air-drying, the Scotch tape was removed and the working electrode was further dried at 393 K for 2 h to improve adhesion.

Photocatalytic Tests for H_2 Production: Photocatalytic H_2 evolution activities were evaluated in a closed system equipped with a pressure detector to examine the pressure of the evolved gases in during photocatalytic reactions. White LED light (50 W $\lambda > 420$ nm), purple LED (50 W $\lambda = 410$ and 420 nm) and blue LED (50 W $\lambda = 465$ nm) was used for photocatalytic H_2 evolution evaluation, respectively. The used volume of the reactor was 38 mL and the temperature was controlled 298 K by cycle water. The evolved amounts of the gases were finally calculated by the Clausius–Clapeyron relation (PV = nRT). Typically, 50 mg of solid catalysts was dispersed into 38 mL of DI water and TEOA (10 vol%) mixture, while they were degassed in advance for use with vacuum and sonication, respectively. 3 wt% of Pt cocatalyst were deposited by a typical in situ photodeposition strategy from H_2PtCl_6 precursor. The H_2 evolution rate was calculated excluding the first reaction hour.

The AQY Measurement and Wavelength Experiment: H_2 evolution AQY was measured using a monochromatic visible light (420 ± 1.0 nm). The AQY was calculated as follows

$$AQY(\%) = \frac{2 \times n_{H_2} \times N_A \times hc}{S \times I \times \lambda} \times 100 \quad (1)$$

where r_{H2} is the production rate of H_2 molecules (mol s^{-1}), N_A is Avogadro constant (6.022×10^{23} mol^{-1}), hc is the Planck constant (6.626×10^{-34} J s^{-1}) multiplied by c the speed of light (3×10^8 m s^{-1}) giving ($1.98644586 \times 10^{-25}$ J m), S is the irradiation area (cm^2), I is the intensity of irradiation light (W cm^{-2}), and λ is the wavelength of the monochromatic light (m).

Supporting Information

Supporting Information is available from the Wiley Online Library or from the author.

Acknowledgements

This research was supported financially by the Max Planck Society. The authors IFT and IFS are grateful to the Brazilian funding agencies CAPES, CNPq (423196/2018-9), and FAPESP (2020/14741-6 and 2021/11162-8) for financial support. I.F.T thanks the Alexander von Humboldt Foundation for his postdoctoral fellowship.

Open access funding enabled and organized by Projekt DEAL.

Conflict of Interest

The authors declare no conflict of interest.

Data Availability Statement

Research data are not shared.

Keywords

carbon nitrides, HER, hydrogen, Na-PHI, photocatalysis, poly(heptazine imide)

Received: November 5, 2021
Revised: December 7, 2021
Published online: January 13, 2022

[1] L. Lin, Z. Lin, J. Zhang, X. Cai, W. Lin, Z. Yu, X. Wang, *Nat. Catal.* **2020**, *3*, 649.
[2] P. Nikolaidis, A. Poullikkas, *Renewable Sustainable Energy Rev.* **2017**, *67*, 597.
[3] a) Y. Li, S. C. E. Tsang, *Mater. Today Sustainability* **2020**, *9*, 100032; b) I. F. Teixeira, E. C. M. Barbosa, S. C. E. Tsang, P. H. C. Camargo, *Chem. Soc. Rev.* **2018**, *47*, 7783.

© 2022 The Authors. Advanced Sustainable Systems published by Wiley-VCH GmbH

[4] W. Yang, R. Godin, H. Kasap, B. Moss, Y. Dong, S. A. J. Hillman, L. Steier, E. Reisner, J. R. Durrant, *J. Am. Chem. Soc.* **2019**, *141*, 11219.
[5] Y. Markushyna, P. Lamagni, C. Teutloff, J. Catalano, N. Lock, G. Zhang, M. Antonietti, A. Savateev, *J. Mater. Chem. A* **2019**, *7*, 24771.
[6] A. Savateev, N. V. Tarakina, V. Strauss, T. Hussain, K. ten Brummelhuis, J. M. Sánchez Vadillo, Y. Markushyna, S. Mazzanti, A. P. Tyutyunnik, R. Walczak, M. Oschatz, D. M. Guldi, A. Karton, M. Antonietti, *Angew. Chem., Int. Ed.* **2020**, *59*, 15061.
[7] M. A. Khan, I. F. Teixeira, M. M. J. Li, Y. Koito, S. C. E. Tsang, *Chem. Commun.* **2016**, *52*, 2772.
[8] I. F. Silva, I. F. Teixeira, R. D. F. Rios, G. M. do Nascimento, I. Binatti, H. F. V. Victória, K. Krambrock, L. A. Cury, A. P. C. Teixeira, H. O. Stumpf, *J. Hazard. Mater.* **2021**, *401*, 123713.
[9] a) M. A. R. da Silva, I. F. Silva, Q. Xue, B. T. W. Lo, N. V. Tarakina, B. N. Nunes, P. Adler, S. K. Sahoo, D. W. Bahnemann, N. López-Salas, A. Savateev, C. Ribeiro, T. D. Kühne, M. Antonietti, I. F. Teixeira, *Appl. Catal., B* **2022**, *304*, 120965; b) F. M. Colombari, M. A. R. da Silva, M. S. Homsi, B. R. L. de Souza, M. Araujo, J. L. Francisco, G. T. S. T. da Silva, I. F. Silva, A. F. de Moura, I. F. Teixeira, *Faraday Discuss.* **2021**, *227*, 306.
[10] X. Fan, L. Zhang, M. Wang, W. Huang, Y. Zhou, M. Li, R. Cheng, J. Shi, *Appl. Catal., B* **2016**, *182*, 68.
[11] a) M. Zhang, X. Bai, D. Liu, J. Wang, Y. Zhu, *Appl. Catal., B* **2015**, *164*, 77; b) Q. Lin, L. Li, S. Liang, M. Liu, J. Bi, L. Wu, *Appl. Catal., B* **2015**, *163*, 135; c) Y. Di, X. Wang, A. Thomas, M. Antonietti, *ChemCatChem* **2010**, *2*, 834; d) Y. Zheng, L. Lin, B. Wang, X. Wang, *Angew. Chem., Int. Ed.* **2015**, *54*, 12868; e) Y. Zheng, L. Lin, B. Wang, X. Wang, *Angew. Chem.* **2015**, *127*, 13060; f) F. K. Kessler, Y. Zheng, D. Schwarz, C. Merschjann, W. Schnick, X. Wang, M. J. Bojdys, *Nat. Rev. Mater.* **2017**, *2*, 17030; g) W.-J. Ong, L.-L. Tan, Y. H. Ng, S.-T. Yong, S.-P. Chai, *Chem. Rev.* **2016**, *116*, 7159; h) Y. Li, X. Li, H. Zhang, J. Fan, Q. Xiang, *J. Mater. Sci. Technol.* **2020**, *56*, 69.
[12] a) G. Zhang, Y. Xu, D. Yan, C. He, Y. Li, X. Ren, P. Zhang, H. Mi, *ACS Catal.* **2021**, *11*, 6995; b) G. Zhang, Y. Xu, C. He, P. Zhang, H. Mi, *Appl. Catal., B* **2021**, *283*, 119636; c) S. K. Sahoo, I. F. Teixeira, A. Naik, J. Heske, D. Cruz, M. Antonietti, A. Savateev, T. D. Kühne, *J. Phys. Chem. C* **2021**, *125*, 13749; d) W. Iqbal, B. Qiu, Q. Zhu, M. Xing, J. Zhang, *Appl. Catal., B* **2018**, *232*, 306; e) W.-C. Lin, S. Wu, G. Li, P.-L. Ho, Y. Ye, P. Zhao, S. Day, C. Tang, W. Chen, A. Zheng, *Chem. Sci.* **2020**, *12*, 210; f) G. Algara-Siller, N. Severin, S. Y. Chong, T. Björkman, R. G. Palgrave, A. Laybourn, M. Antonietti, Y. Z. Khimyak, A. V. Krasheninnikov, J. P. Rabe, *Angew. Chem., Int. Ed.* **2014**, *53*, 7450; g) L. Lin, C. Wang, W. Ren, H. Ou, Y. Zhang, X. Wang, *Chem. Sci.* **2017**, *8*, 5506.
[13] R. Godin, Y. Wang, M. A. Zwijnenburg, J. Tang, J. R. Durrant, *J. Am. Chem. Soc.* **2017**, *139*, 5216.
[14] V. W.-h. Lau, D. Klose, H. Kasap, F. Podjaski, M. C. Pignié, E. Reisner, G. Jeschke, B. V. Lotsch, *Angew. Chem.* **2017**, *129*, 525.
[15] V. W.-h. Lau, I. Moudrakovski, T. Botari, S. Weinberger, M. B. Mesch, V. Duppel, J. Senker, V. Blum, B. V. Lotsch, *Nat. Commun.* **2016**, *7*, 12165.
[16] a) B. V. Lotsch, W. Schnick, *Chem. Mater.* **2006**, *18*, 1891; b) D. Dontsova, S. Pronkin, M. Wehle, Z. Chen, C. Fettkenhauer, G. Clavel, M. Antonietti, *Chem. Mater.* **2015**, *27*, 5170.
[17] P. Makuła, M. Pacia, W. Macyk, *J. Phys. Chem. Lett.* **2018**, *9*, 6814.
[18] X. Wang, K. Maeda, A. Thomas, K. Takanabe, G. Xin, J. M. Carlsson, K. Domen, M. Antonietti, *Nat. Mater.* **2009**, *8*, 76.
[19] a) G. Zhang, G. Li, Z. A. Lan, L. Lin, A. Savateev, T. Heil, S. Zafeiratos, X. Wang, M. Antonietti, *Angew. Chem.* **2017**, *129*, 13630; b) G. Zhang, L. Lin, G. Li, Y. Zhang, A. Savateev, S. Zafeiratos, X. Wang, M. Antonietti, *Angew. Chem., Int. Ed.* **2018**, *57*, 9372.
[20] Y. Markushyna, C. Teutloff, B. Kurpil, D. Cruz, I. Lauermann, Y. Zhao, M. Antonietti, A. Savateev, *Appl. Catal., B* **2019**, *248*, 211.
[21] W. Xu, X. Zhao, X. An, S. Wang, J. Zhang, Z. Li, W. Wu, M. Wu, *ACS Appl. Mater. Interfaces* **2020**, *12*, 48526.
[22] R. Subbaraman, D. Tripkovic, D. Strmcnik, K.-C. Chang, M. Uchimura, A. P. Paulikas, V. Stamenkovic, N. M. Markovic, *Science* **2011**, *334*, 1256.
[23] M. M. Waegele, C. M. Gunathunge, J. Li, X. Li, *J. Chem. Phys.* **2019**, *151*, 160902.

© 2022 The Authors. Advanced Sustainable Systems published by Wiley-VCH GmbH